Segmentation of Breast Nodules on Ultrasonographic Images Based on Marke d-Controlled Watershed Transform

Segmentación de Nódulos Mamarios en Imágenes Ultrasonográficas Basado en Transformada Watershed Controlada por Marcadores

W. Gómez[1], L. Leija[1], W. C. A. Pereira[2] and A. F. C. Infantosi[2]
[1]Department of Electrical Engineering, CINVESTAV-IPN, Mexico City, Mexico
wgomez@cinvestav.mx
[2]Biomedical Engineering Program - COPPE/UFRJ, Rio de Janeiro, Brazil
wagner@peb.ufrj.br

Article received on January 07, 2009; accepted on October 01, 2009

Abstract. In this article is presented a computerized segmentation method for breast nodules on ultrasonic images. With the goal of removing the speckle while preserving important information from the lesion boundaries, a Gabor filter followed by an anisotropic diffusion filtering are applied to the ultrasonic image. Furthermore, the marker-controlled Watershed transform defines potential boundaries that maximize the Average Radial Derivative function to get the final lesion contour. The segmentation procedure was applied on a database of 50 images and the computer-delineated margins were compared against manual outlines drawn by two radiologist. This comparison was performed by two metrics, which measure the similarity between two compared images: overlap ratio (OR) and normalized residual value (nrv). If there is perfect agreement between both images OR = 1 and nrv = 0. Then, the mean values results, for each metric, were for the first radiologist: OR = 0.87±0.04 and nrv = 0.14±0.06, and for the second radiologist: OR = 0.86±0.06 and nrv = 0.15±0.05.
Keywords: Breast ultrasound, Segmentation, Watershed transform, Average radial derivative.

Resumen. En este trabajo se presenta un método computacional para la segmentación de nódulos mamarios en imágenes ultrasónicas. Con el objetivo de remover el ruido multiplicativo (*speckle*) mientras se preservan los detalles importantes del contorno del tumor, se aplica un filtro de Gabor seguido de un filtro de difusión anisotrópico sobre la ultrasonografía de mama. Posteriormente, la transformada *Watershed* (línea divisora de aguas) controlada por marcadores define bordes potenciales que maximizan la Media Radial Derivativa para encontrar el contorno final de la lesión. El procedimiento de segmentación se aplicó en un banco de 50 ultrasonografías y la segmentación computarizada obtenida de cada imagen fue comparada contra las delineaciones manuales realizadas por dos radiólogos. Dicha comparación fue cuantificada a través de dos métricas, los cuales miden la similitud entre las imágenes comparadas: razón de superposición (OR) y valor residual normalizado (nrv). En el caso de coincidencia perfecta entre ambas imágenes OR = 1 y nrv = 0. Los valores promedio de cada métrica fueron para el primer radiólogo: OR = 0.87±0.04 y nrv = 0.14±0.06, y para el segundo radiólogo: OR = 0.86±0.06 y nrv = 0.15±0.05.
Palabras clave: Ultrasonido de mama, Segmentación, Transformada *Watershed*, Media radial derivativa.

1 Introduction

Early diagnosis is a crucial factor in breast cancer treatment and medical imaging is a very powerful assessment tool. Nowadays, breast ultrasound (US) is accepted as the most important adjunct to mammography for patients with palpable nodules and normal or inconclusive mammograms. It is particularly useful in distinguishing cystic from non-cystic (solid) breast lesions [Zonderland *et al.*, 1999].

Malignant tumors generally infiltrate the surrounding tissue and they present several morphological features associated to malignancy such as: (a) spiculation, a distortion caused by the intrusion of the breast cancer into the surrounding tissue [Huang *et al.*, 2004]; (b) angular margins, obtuse or acute pointed junctions between the mass and surrounding tissue; and (c) microlobulation, that is frequently associated with angular margins and is characterized by greater than three lobulations of the mass surface [Chang *et al.*, 2005]. Therefore, analyzing the lesion contour morphology it is

possible to give a diagnostic hypothesis about the tumor malignancy.

However, due to the large overlap in the sonographic appearance of breast nodules, it has been difficult to diagnose them as benign or malignant only by visual inspection of the specialist [Giger, 2000]. To improve diagnosis, several researchers have been developed quantitative methods to build computer-aided diagnosis (CAD) systems [Alvarenga *et al.*, 2003; Horsch *et al.*, 2001; Infantosi *et al.*, 2008].

In a CAD system, the accurate segmentation of breast lesions in US images is a difficult task since presence of speckle noise and shadows, the low or non-uniform contrast of certain structures, and the variability of the echogenicity of the nodules [Alemán-Flores *et al.*, 2007]. Thus, to obtain segmentation which can be used for diagnosis depends on two aspects: (1) image pre-processing and (2) gray-level threshold selection.

The computerized segmentation techniques could be classified in two categories: edge-based techniques, that look for edges between regions with different characteristics, and region-based techniques, that cluster image regions that satisfy a given homogeneity criterion [Bankman, 2000]. Edge-based segmentation methods depend on the image gradient to determine the boundary of an object.

These methods do not achieve a good performance when the US image presents weak defined edges or large amount of speckle that produces spurious edges [Huang & Chen, 2004]. On the other hand, region-based segmentation methods, such as region-growing [Drukker *et al.*, 2002; Horsch *et al.*, 2001; Oshiki *et al.*, 2004], snake-deformation [Alemán-Flores *et al.*, 2007; Chang *et al.*, 2005; Chen *et al.*, 2000], split-and-merge [Chen *et al.*, 2005; Cheng *et al.*, 2007], and morphological watershed transformation [Huang & Chen, 2004] have been widely explored for segmenting breast US images.

In this study, we propose a region-based segmentation technique applied to breast ultrasound. This method employs a Gabor filter followed by an anisotropic diffusion filter to reduce speckle without losing important information about lesions boundaries and detailed structures. After that, a constraint Gaussian function is multiplied by the filtered image to attenuate objects that have the same gray-levels as the lesion region but do not belong to it. Next, a region-growing scheme, based on a gray-level thresholding procedure of the preprocessed image, defines binary partitions. With those binary images are created markers used as the set of minima to impose to the segmentation function (image gradient) to control the flooding of Watershed transformation, in order to obtain accurate potential lesion margins. Each potential contour evaluates the Average Radial Derivative (ARD) function, which measures the gray-level gradients along the margin. The argument of the maximum of the ARD curve defines the index of the final lesion contour, i.e., in that contour there is the maximum gray-level gradient between the lesion region and its background.

2 Material and Methods

2.1 Image Database

In this study, using a 7.5–MHz linear array B-mode 40-mm ultrasound probe (Sonoline–Sienna® Siemens) 50 ultrasonographies were acquired at the Cancer National Institute (Rio de Janeiro, Brazil), during routine studies. For each image, two experienced radiologists determined a rectangular Region-of-Interest (ROI) including the tumor and healthy tissue around it. Besides, the same two radiologists delineated manually all tumor contours using software designed for that purpose.

2.2 Speckle Filtering

There are several fundamental requirements for medical image filtering. First, it should preserve the important information from lesion boundaries and detailed structures; second, it should efficiently suppress the noise in homogenous regions; and third, it should enhance the edge information [Gerig *et al.*, 1992]

Ultrasonic images are characterized by speckle artifact, which degrades the image by concealing fine structures and reducing the signal to noise ratio (SNR) [Yu & Acton, 2002]. Moreover, in many cases, it is harder to locate the edges of different elements due to the low contrast between the structures to be segmented and the background. Therefore, it is necessary to remove speckle and enhance the edges among distinct regions before the segmentation procedure.

With conventional spatial filters applied to remove speckle in breast US, such as median

[Horsch *et al.*, 2001], truncated median [Alemán-Flores *et al.*, 2003], Wiener [Huang & Chen, 2004], the price paid for removing the noise is the blurring of lesion edges. Anisotropic diffusion is a non-linear filtering method, which tries to reduce the speckle of the image whereas preserving the contrast of the lesion edges, that means, the contour of the objects are slightly modified by the diffusion process [Alemán-Flores *et al.*, 2007]. The anisotropic diffusion equation is given as follows [Perona & Malik, 1990]:

$$I_t = \mathrm{div}\left[c\left(\|\nabla I\|\right)\nabla I\right], \tag{1}$$

where ∇ is the gradient operator, div is the divergence operator, I is the initial 2D image, $\|-\|$ denotes the magnitude, and $c(\cdot)$ is the diffusion coefficient that enhances wide regions over smaller ones, and it is expressed as

$$c\left(\nabla I\right) = \frac{1}{1+\left(\frac{\|\nabla I\|}{\kappa}\right)^2}, \tag{2}$$

where the constant κ is a parameter to control the diffusion extension.

Anisotropic diffusion works properly in many kinds of images, mainly when the objects have uniform intensity regions. However, in the case of US images, it is important to express similarity between different areas in terms of texture descriptors instead of intensities.

The input image $I(x,y)$ is assumed to be composed of disjoint regions of $N > 2$ different textures. Then, $I(x,y)$ is filtered with a bandpass Gabor filter with spatial impulse response $h(x,y)$:

$$h(x,y) = \frac{1}{2\pi\sigma_g^2}\cdot \exp\left(-\frac{x^2}{2\pi\sigma_g^2}\right)\cdot \cos\left(k_x x^2 + k_y y^2\right), \tag{3}$$

The Gabor function $h(x,y)$ is a sinusoid centered at the frequency (k_x,k_y) and modulated by a Gaussian envelope. The parameter σ_g determines the scale of the envelope of $h(x,y)$ [Weldon *et al.*, 1996]. The output of the Gabor filter is calculated as the convolution in two dimensions of the original ROI with the filter response defined in (3). Then, the resultant image is the input of the anisotropic diffusion filter depicted in (1) to obtain the despeckled image with enhanced edges, $\tilde{I}$. In Fig. 1(b), are illustrated the result of applying the speckle filtering on a breast US containing an irregular lesion shown in Fig. 1(a).

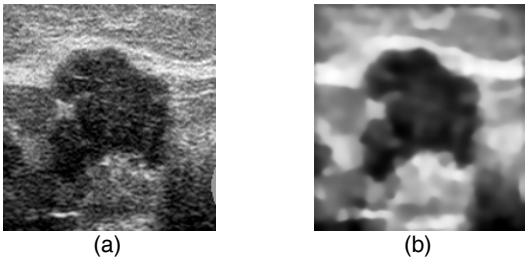

(a) (b)

Fig. 1. (a) Original ROI image of an irregular breast lesion with rounded and angular margins, diffuse edges, concavities and non-uniform intensity. (b) Despeckled image by applying Gabor filter followed by anisotropic diffusion filtering

2.3 Constraint Gaussian Function

The next step involves multiplying the complement of the filtered image, $\tilde{I}$, by a constraint Gaussian function, $C(\hat{P})$, positioned on the lesion center. The purpose is to attenuate distant pixels that have gray-level values similar to the tumor region. Then, the resultant image has higher gray values in the region of the lesion and gray values near to zero far from the lesion [Horsch *et al.*, 2001] (Fig. 2).

The multiplication of the inverted filtered image by the Gaussian function is defined as [Fig. 3(a)]

$$J(\hat{P}) = C(\hat{P})\cdot\left(1 - \frac{\tilde{I}(\hat{P})}{max_{\hat{P}}\left(\tilde{I}(\hat{P})\right)}\right) \tag{4}$$

where $\hat{P}$ is the pixel location and the constraint Gaussian function, $C(\hat{P})$, is expressed as

$$C(\hat{P}) = \frac{\exp\left(-\frac{1}{2}\left(\frac{(\hat{P}-\hat{\mu})^2}{\sigma_x^2} + \frac{(\hat{P}-\hat{\mu})^2}{\sigma_y^2}\right)\right)}{2\pi\sqrt{\det S_\sigma}}, \tag{5}$$

where $\hat{\mu}$ is the lesion center coordinates, and K is a matrix with the variances in the horizontal and vertical directions, $\sigma_x = w/2$ and $\sigma_y = h/2$, where w and h are the lesion width and height, respectively, which are estimated manually by the user.

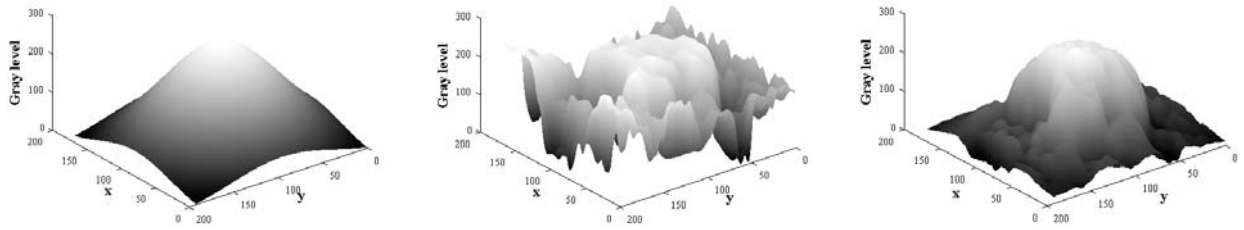

Fig. 2. Effect of the constraint Gaussian function where the z-axis represents the image gray-levels. (a) Constraint Gaussian function. (b) Negative of the filtered image where it is observed structures that do not belong to the tumor but have similar gray-levels. (c) By multiplying (a) and (b) the lesion region is enhanced and those distant structures are attenuated

2.4 Watershed transformation

The Watershed transform is the first option for image segmentation in the field of Mathematical Morphology, and can be classified as a region-based segmentation approach. Its principle can be understood from an intuitive idea coming from Geography. Let's imagine a landscape or topographic relief immersed progressively in a lake, with holes pierced in its local minima. Basins (also called "catchment basins") will fill up with water beginning from these local minima. Then, at points where water coming from different basins meets, dams are built. When the water level has reached the highest peak in the landscape, the process is halted. As a result, the landscape is divided into regions or basins separated by dams, called watershed lines or simply watersheds [Parvati *et al.*, 2008; Roerdink & Meijster, 2001; Vincent & Soille, 1991]. In practice, a direct computation of the Watershed transform on the image to be segmented (segmentation function) produces an over-segmentation, which is due to the presence of spurious minima. Therefore, the segmentation function must be filtered by minima imposition technique in order to remove all irrelevant minima. This technique requires the determination of a marker function to point the relevant structures within the image to control the flooding only to the catchment basins associated to each marker. This technique is known as marker-controlled watershed transformation (MCWT) and it is a robust and flexible method for segmenting objects with closed contours (e.g. breast lesions), where the boundaries are expressed as ridges [Parvati *et al.*, 2008; Soille, 2004].

2.4.1 Segmentation Function

The determination of the segmentation function is based on a model for the definition of an object boundary. The lesion region within the image $J(\hat{P})$ (defined in Eq. 4) presents rather constant gray level values. By computing the gradient operator the lesion boundaries will be enhanced. Then, by using a set of eight Newton filters (Table 1) the preprocessed image $J(\hat{P})$ is filtered, which enhance the lesion edges according to their orientations [Alemán-Flores *et al.*, 2001].

Table 1. Set of eight Newton filter kernels and their corresponding orientations

$F_0 = \begin{pmatrix} +1 & +1 & -2 \\ +2 & +2 & -4 \\ +1 & +1 & -2 \end{pmatrix}$	$F_1 = \begin{pmatrix} +1 & -2 & -4 \\ +1 & +2 & -2 \\ +2 & +1 & +1 \end{pmatrix}$
F_0: 0	F_1: $\pi/4$
$F_2 = \begin{pmatrix} -2 & -4 & -2 \\ +1 & +2 & +1 \\ +1 & +2 & +1 \end{pmatrix}$	$F_3 = \begin{pmatrix} -4 & -2 & +1 \\ -2 & +2 & +1 \\ +1 & +1 & +2 \end{pmatrix}$
F_2: $\pi/2$	F_3: $3\pi/4$
$F_4 = \begin{pmatrix} -2 & +1 & +1 \\ -4 & +2 & +2 \\ -2 & +1 & +1 \end{pmatrix}$	$F_5 = \begin{pmatrix} +1 & +1 & +2 \\ -2 & +2 & +1 \\ -4 & -2 & +1 \end{pmatrix}$
F_4: π	F_5: $5\pi/4$
$F_6 = \begin{pmatrix} +1 & +2 & +1 \\ +1 & +2 & +1 \\ -2 & -4 & -2 \end{pmatrix}$	$F_7 = \begin{pmatrix} +2 & +1 & +1 \\ +1 & +2 & -2 \\ +1 & -2 & -4 \end{pmatrix}$
F_6: $3\pi/2$	F_7: $7\pi/4$

The segmentation function is determined by calculating the magnitude of the image $J(\hat{P})$ convolving by the eight Newton filters defined as [Fig. 3(b)]

$$f_s = \sqrt{\sum_i \left(F_i * J(\hat{P})\right)^2}\,, \tag{6}$$

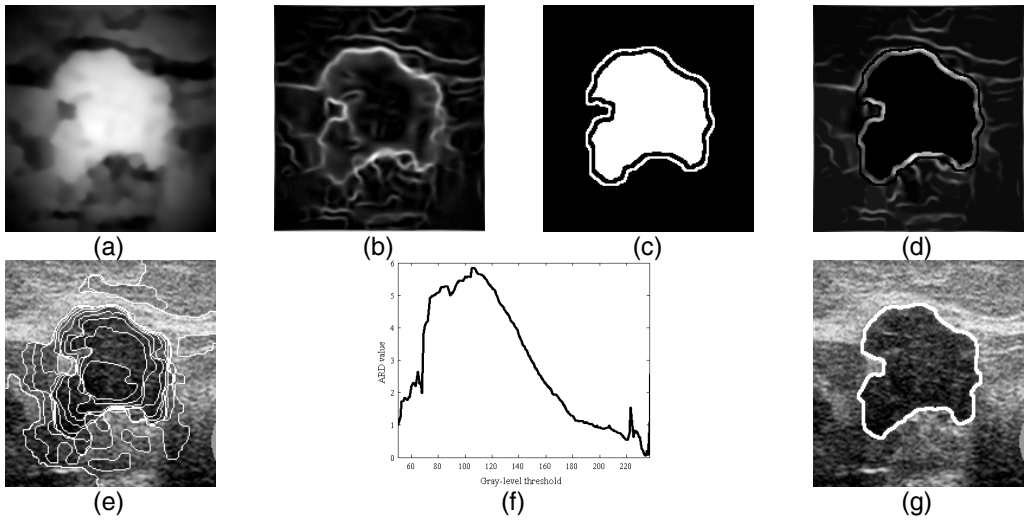

Fig. 3. (a) Inverted filtered image multiplied by the constraint Gaussian function. (b) Segmentation function derived from the set on Newton filters. (c) Marker function computed by morphological operators defined at gray-level threshold *th* = 115 of (a). (d) Minima imposition of the marker function on the segmentation function at *th* = 115. (e) Potential lesion margins computed by Watershed transformation over the imposed image for several thresholds. (f) Average radial derivative curve. It is observed a maximum at *th* = 115, where exists the maximum gradient between the lesion and its background. (g) Segmented lesion defined by the potential lesion margin that maximizes de ARD at *th* = 115

where F_i is the Newton filter with a specific orientation $i = 0,1,\ldots,7$, as illustrated in Table 1, and $*$ is the convolution operator.

2.4.2 Marker Function

Gray-level thresholding (*th*) from 0 to 255 of $J(\hat{P})$ image defined binary partitions that are used to create both external and internal markers. The external marker is calculated by the morphological Beucher gradient (structuring element -SE- square 3×3 pixels) of binary partition dilation (SE disk, 5 pixels radius), whereas the internal marker is computed by eroding the binary partition (SE disk, 3 pixels radius). The logical union of the internal and external markers determines the function marker [Fig. 3(c)] and is used as the set of minima to impose to the segmentation function.

2.4.3 Potential lesion margins

When the image $J(\hat{P})$ is thresholded to create the marker function, it is obtained a set of segmented images defining "lesion-like" shapes. However, $J(\hat{P})$ is a distorted version of the constraint Gaussian function, produced by the multiplication with the inverted filtered image. Therefore, when the lesion shape is highly irregular, the binary partition will not track accurately the tumor contour, because it does not take into account the image gradient information, adding structures that do not belong to the lesion.

To solve this, the minima imposition of the marker function over the segmentation function is used to guarantee that the gradient information is contained between the internal and external markers, while removing all irrelevant minima [Fig. 3(d)]. Then, a potential lesion margin is obtained by computing the Watershed transformation of the

minima imposed image at each gray-level threshold [Fig. 3(e)].

Because the $J(\hat{P})$ is thresholded from 0 to 255 gray-levels, it is created a set of 256 potential lesion margins. In order to select one of them as the final lesion contour, the Average Radial Derivative (ARD) function is evaluated by using the information of a potential lesion contour f_{WS}^{th}, in a specific gray-level threshold *th*, and the gradient of the despeckled image $\tilde{I}$ [Fig. 3(f)]. The ARD gives the average directional derivative in the radial direction along the contour and is defined as [Horsch *et al.*, 2001]

$$ARD(f_{WS}^{th}) = \frac{1}{N}\sum_{P \in \widehat{f_{WS}^{th}}} \nabla \tilde{I}\left(\hat{P}\right) \cdot \hat{r}\left(\hat{P}\right) \qquad (7)$$

where f_{WS}^{th} is the discretized potential lesion margin at specific gray-level threshold *th*, *N* is the number of points in f_{WS}^{th}, $\hat{r}(\hat{P})$ is the unit vector in the radial direction from the geometric center of the contour to the point $\hat{P} = (x, y)$, and $\cdot$ is the dot product between vectors. Then, the potential margin, f_{WS}^{th}, that maximizes the ARD function defines the lesion boundary at the gray-level threshold *th* = 0, 1,…, 255 [Fig. 3(g)]. In Fig. 4 is illustrated the pipeline of the proposed segmentation algorithm.

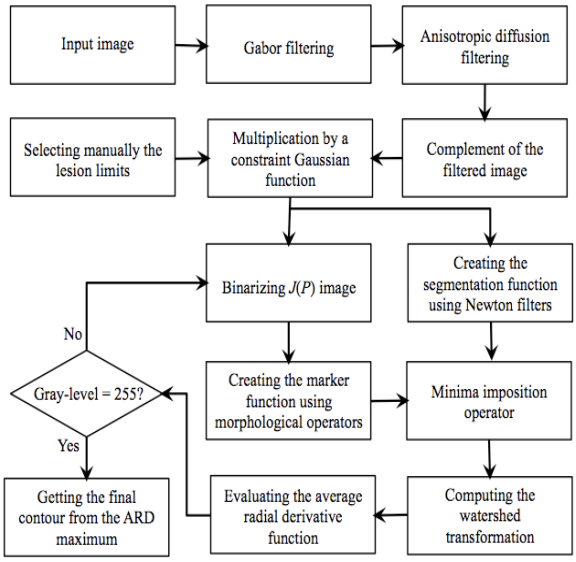

Fig. 4. Pipeline of the proposed segmentation algorithm

2.5 Performance Evaluation

To assess the segmentation algorithm, it was used the database of 50 breast US images. By comparing the binary computer-delineated images against the radiologists' manual outlines, it is possible to measure the agreement between contours. This quantification was performed by two parameters: overlap ratio (OR) and normalized residual value (nrv). Both metrics require two binary images for the same lesion: S_C (computerized segmentation) and S_R (radiologist's outline).

Then, the OR parameter is defined by [Horsch *et al.*, 2001]:

$$\mathrm{OR} = \frac{\mathrm{Area}(S_C \cap S_R)}{\mathrm{Area}(S_C \cup S_R)}, \qquad (8)$$

where the symbols $\cap$ and $\cup$ indicate the areas intersection and union, respectively. So, when both images have perfect agreement OR is equal to unity.

The parameter nrv takes into account the relative positions of pixels that depict the object contour; and can be expressed as [Infantosi *et al.*, 1998]

$$\mathrm{nrv} = \frac{\mathrm{Area}(S_C \oplus S_R)}{\mathrm{Area}(S_R)}, \qquad (9)$$

where $\oplus$ represents an exclusive-or operation. Hence, if S_C and S_R are congruent, nrv = 0.

2.6 Comparison with Horsch's method

In order to compare the performance of our segmentation technique, it was also implemented the method proposed by Horsch *et al.* (2001). In that work, the authors applied the constraint Gaussian function to breast US, and to select the final lesion contour they maximized the ARD function. As depicted previously, both stages are part of our segmentation technique. However, we tried to improve the segmentation method by adding other techniques, such as anisotropic diffusion and watershed transformation, to track more accurately the lesion contour. There were used the parameters OR and nrv to measure the Horsch's method performance. The nomenclature to differentiate the results of both techniques is SM_W for our

segmentation method and SM_H for Horsch's technique.

3 Results

In Fig. 5 are illustrated some examples of both methods (SM_W and SM_H) applied on breast US containing irregular lesions. As observed, both computerized segmentation methods delineated the lesions with some differences between them and in relation to radiologist's outlines. SM_H tends to smooth the lesion contour and, in some cases, adds to segmentation tissue that does not belong to lesion. This effect is due to the median filter (10×10 pixels) used by SM_H, which blurs the image and, consequently, loses the steep gray-level discontinuities. On the other hand, SM_W depicted more accurately the details on the lesion boundaries, because of the combination of different filtering techniques, such as Gabor filter and anisotropic diffusion. This ability is important to extract relevant information for classification purposes.

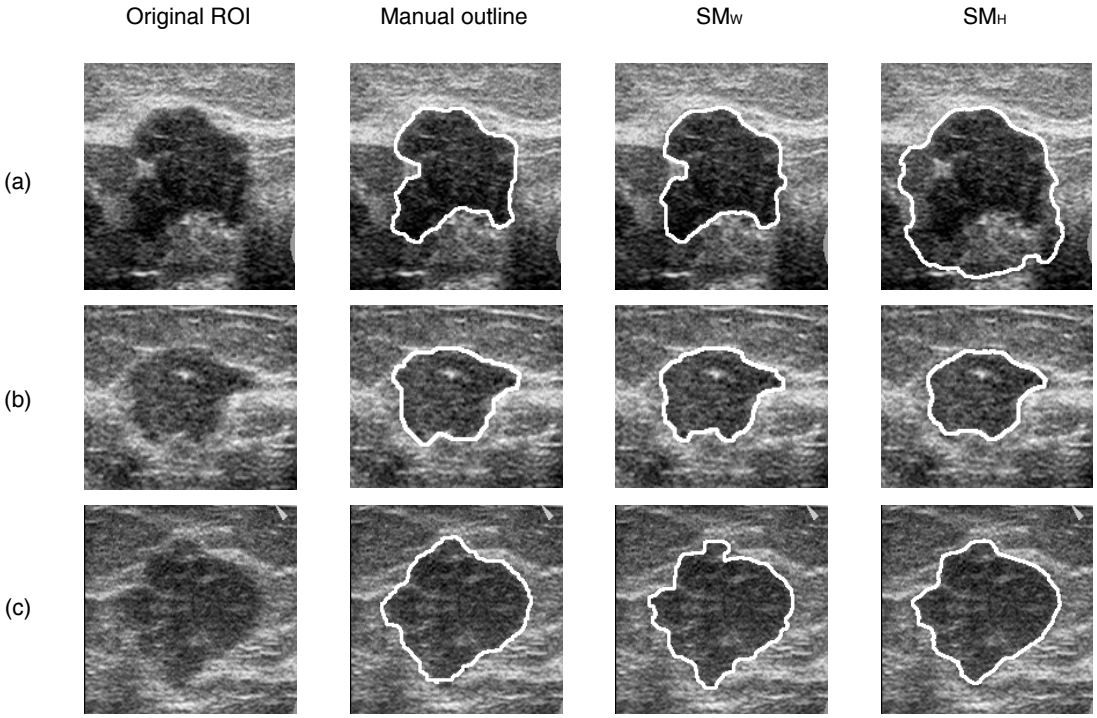

Fig. 5. Examples of both manual delineation and computerized segmentations (SM_W and SM_H). The three lesions have irregular shapes that combine rounded and angular margins diffuse edges, concavities and non-uniform intensity. The differences presented between SM_W and SM_H in relation to the manual outlines is mainly due to the filtering method and the technique to define potential margins

In the case of radiologist's outlines, it is noticeable that the specialist could not follow little details on lesion contours. Therefore, the advantage in using computerized segmentation is that avoids human variability.

The graphs in Fig. 6 show the results for the two parameters, OR and nrv, for the entire database. The curve notations are as follows: R1×R2 is the comparison between both radiologists delineations (reference); SM_W×R1 and SM_W×R2 are the comparisons between SM_W and manual delineations, and SM_H×R1 and SM_H×R2 refers to the Horsch's segmentation with respect to the radiologists outlines.

If it is taken any threshold value (*x*-axis), for both metrics OR and nrv, it is found the percentage of

images (*y*-axis) that reached that threshold. For example, in order to compare the performance between SM_W and SM_H we could define the following threshold values: OR = 0.8 and nrv = 0.2. Therefore, the method that achieves the largest percentage of images has the best performance (Table 2).

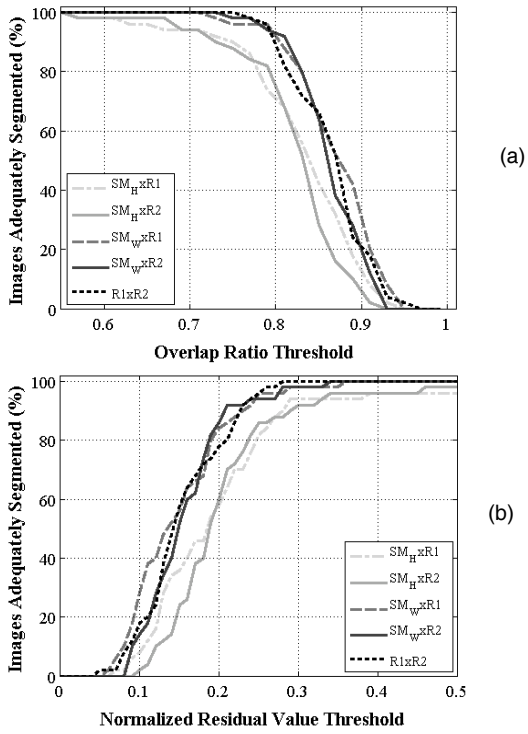

Fig. 6. Percentage of images segmented at different thresholds using the proposed technique (SM_W) and Horsch technique (SM_H) for (a) overlap ratio and (b) normalized residual value, for which computerized segmentations and the manual delineations respectively agree

Table 2. Percentage of images that reached the threshold values of OR = 0.8 and nrv = 0.2 for SM_W and SM_H.

Test	SM_W		SM_H	
	OR = 0.8	nrv = 0.2	OR = 0.8	nrv = 0.2
R1	94%	84%	70%	58%
R2	94%	86%	78%	60%

The results summarized in Table 2 pointed out that our segmentation technique delineates the lesion contour accurately in relation to radiologists' reference.

In Table 3 are enlisted the mean values of the metrics OR and nrv applied to the entire database, by using as reference both radiologists' outlines. These results confirm that our algorithm presented an improvement in relation with SM_H.

Table 3. Mean values for the metrics OR and nrv to quantify the performance of $SM_W$and SM_H

Test	SM_W		SM_H	
	OR	nrv	OR	nrv
R1	0.87±0.04	0.14±0.06	0.82±0.07	0.20±0.11
R2	0.86±0.06	0.15±0.05	0.81±0.06	0.20±0.10

4 Conclusions

In this article was presented a segmentation method for breast lesions on US images. This technique preprocess the image with a Gabor filter followed by an anisotropic diffusion filtering, in order to preserve and enhance useful information in the lesion boundaries, unlike from other filtering techniques that blur the image, such as median filter used in Horsch's method.

The constraint Gaussian function plays an important role within the segmentation algorithm, because it attenuates undesired structures with similar gray-levels that the lesion region. This stage prepares the image for the region-growing procedure, performed by the image thresholding, from 0 to 255, to create "lesion–like" shapes. After that, each partition is used to create markers that are placed within the desired regions to be segmented. This procedure controls watershed transformation only to the regions associated to each marker. Then, potential lesion margins are created and the ARD function is maximized to get the final lesion contour. The combination of these techniques provides quite satisfactory results in the segmentation of complex images such as ultrasonographies.

Marker-controlled watershed transformation is defined as a robust and flexible method for segmenting objects with closed contours, such as breast nodules. Besides, its functioning is improved when is combined with the region-growing procedure, derived from the thresholding of the filtered image multiplied by constraint Gaussian function to find potential lesion margins. One advantage of our method is its simplicity to be implemented, because it does not require large

computational cost to solve complex mathematical models, such as snake-deformation.

Encouraged by these results, our current efforts are to include this technique as part of the development of a CAD system to give support to the detection and diagnose of breast lesions on US images.

Acknowledgments

To Consejo Nacional de Ciencia y Tecnología (CONACYT, Mexico) and the Brazilian National Research Council – CNPq (Brazil) for the financial support.

References

1. **Alemán-Flores, M., Alemán-Flores, P., Álvarez-León, L., Santana-Montesdeoca, J. M., Fuentes-Pavón, P., & Trujillo-Pino, A. (2003).** Computational techniques for the support of breast tumor diagnosis on ultrasound images. Cuadernos del Instituto Universitario de Ciencias y Tecnologías Cibernéticas, ULPGC 27, 1-12.
2. **Alemán-Flores, M., Álvarez, L., & Caselles, V. (2007).** Texture-oriented anisotropic filtering and geodesic active contours in breast tumor ultrasound segmentation. Journal of Mathematical Imaging and Vision, 28(1), 81-97.
3. **Alemán-Flores, M., Álvarez, L., & Moreno, R. (2001).** Modified Newton filters for edge orientation estimation and shape representation. IASTED International Conference on Signal Processing, Pattern Recognition & Applications. Rhodes, Greece, 27-32.
4. **Alvarenga, A. V., Infantosi, A. F. C., Azevedo, C. M., & Pereira, W. C. A. (2003).** Application of morphological operators on the segmentation and contour detection of ultrasound breast images. Brazilian Journal on Biomedical Engineering, 19(2), 91-101.
5. **Bankman, I. N. (2000).** Handbook of Medical Imaging: Processing and Analysis. San Diego: Academic Press.
6. **Chang, R. F., Wu, W. J., Moon, W. K., & Chen, D. R. (2005).** Automatic ultrasound segmentation and morphology based diagnosis of solid breast tumors. Breast Cancer Research and Treatment, 89(2), 179-185.
7. **Chen, C. M., Chou, Y. H., Chen, C. S., Cheng, J. Z., Ou, Y. F., Yeh, F. C., & Chen, K. W. (2005).** Cell-competition algorithm: a new segmentation algorithm for multiple objects with irregular boundaries in ultrasound images. Ultrasound in Medicine & Biology, 31(12), 1647-1664.
8. **Chen, C. M., Lu, H. H., & Lin, Y. C. (2000).** An early vision-based snake model for ultrasound image segmentation. Ultrasound in Medicine & Biology, 26(2), 273-285.
9. **Cheng, J. Z., Chen, C. M., Chou, Y. H., Chen, C. S., Tiu, C. M., & Chen, K. W. (2007).** Cell-based two-region competition algorithm with a map framework for boundary delineation of a series of 2D ultrasound images. Ultrasound in Medicine & Biology, 33(10), 1640-1650.
10. **Drukker, K., Giger, M. L., Horsch, K., Kupinski, M. A., Vyborny, C. J., & Mendelson, E. B. (2002).** Computerized lesion detection on breast ultrasound. Medical Physics, 29(7), 1438-1446.
11. **Gerig, G., Kubler, O., Kikinis, R., & Jolesz, F. A. (1992).** Nonlinear anisotropic filtering of MRI data. IEEE Transactions on Medical Imaging, 11(2), 221-232.
12. **Giger, M. L. (2000).** Computer-aided diagnosis of breast lesions in medical images. Computing in Science & Engineering, 2(5), 39-45.
13. **Horsch, K., Giger, M. L., Venta, L. A., & Vyborny, C. J. (2001).** Automatic segmentation of breast lesions on ultrasound. Medical Physics, 28(8), 1652-1659.
14. **Huang, S. F., Chang, R. F., Chen, D. R., & Moon, W. K. (2004).** Characterization of spiculation on ultrasound lesions. IEEE Transactions on Medical Imaging, 23(1), 111-121.
15. **Huang, Y. L. & Chen, D. R. (2004).** Watershed segmentation for breast tumor in 2-D sonography. Ultrasound in Medicine & Biology, 30(5), 625-632.
16. **Infantosi, A. F. C., Luz, L. M. S., Pereira, W. C. A., & Alvarenga, A. V. (2008).** Breast ultrasound segmentation using morphologic operators and a Gaussian function constraint. 14th Nordic-Baltic Conference on Biomedical Engineering and Medical Physics, Riga, Latvia, 20, 520-523.
17. **Infantosi, A. F. C., Silva, J. L., Tierra-Criollo, C. J., & Simpson, D. M. (1998).** Avaliação do desempenho de técnicas de interpolação no mapeamento cerebral utilizando simulação. RBE Caderno de Engenharia Biomédica, 14(2), 71-96.
18. **Oshiki, M., Shinomura, R., Mitake, T., Sakurai, T., Matsuura, S., & Harada, J. (2004).** Boundary Detection Method for Ultrasound Diagnostic Images Using Region-Growing Approach, Japanese Journal of Applied Physics, 43(7A), 4411-4416.
19. **Parvati, K., Rao, B. S. P., & Das, M. M. (2008).** Image segmentation using gray-scale morphology and marker-controlled watershed transformation. Discrete Dynamics in Nature and Society, 2008, 1-8.
20. **Perona, P. & Malik, J. (1990).** Scale-space and edge detection using anisotropic diffusion. IEEE Transactions on Pattern Analysis and Machine Intelligence, 35(10), 629-639.
21. **Roerdink, J. & Meijster, A. (2001).** The watershed transform: definitions, algorithms and parallelizations strategies. Fundamenta Informaticae, 41(1-2), 187-228.
22. **Soille, P. (2004).** Morphological Image Analysis: Principles and Applications. 2nd ed. Berlin: Springer-Verlag.
23. **Vincent, L. & Soille, P. (1991).** Watersheds in digital spaces: an efficient algorithm based on immersion simulations. IEEE Transactions on Pattern Analysis and Machine Intelligence, 13(6), 583-598
24. **Weldon, T., Higgins, W. E., & Dunn, D. F. (1996).** Gabor filter design for multiple texture segmentation. Optical Engineering, 35(10), 2852-2863.
25. **Yu, Y. & Acton, S. T. (2002).** Speckle reducing anisotropic diffusion. IEEE Transactions on Medical Imaging, 11(11), 1260-1270.

26. Zonderland, H. M., Coerkamp, E. G., Hermans, J., Van de Vijver, M. J., & van Voorthuisen, A. E. (1999). Diagnosis of breast cancer: contribution of US as an adjunct to mammography. Radiology, 213(2), 413-422.

Wilfrido Gómez Flores

Was born in Mexico City (Mexico) in 1980. In 2004, he received the B.S. degree in Electronic and Communications Engineering from the Universidad Tecnológica de México. He obtained his M.Sc (2006) and D.Sc. (2009) degrees in Electrical Engineering at the Centro de Investigación y de Estudios Avanzados del IPN. He collaborates actively with the Universidade Federal do Rio de Janeiro at the Ultrasound Laboratory (LUS/PEB/COPPE). His main research fields of interest are Computer Vision and Pattern Recognition, Biomedical Ultrasound, Signal Processing and Bioinstrumentation.

Lorenzo Leija Salas

Was born in San Luis Potosí, México, in 1953. He received the Ph.D. degree in Bioengineering (1989) from the Nancy University, France. Currently, he is SNI 2. He has over 30 articles in indexed ISI review and other leading journals, and more than 100 publications in international conferences. He is member of international organizations such as the Biomedical Engineering IEEE-EMBS, AIUM, SOMIB and others. He has dozen books compiled for research and teaching, and several book chapters from recognized publishers. He has supervised 10 Ph.D. thesis and 32 masters. He has coordinated and participated in 8 projects with international funding.

Wagner Coelho de Albuquerque Pereira

Was born in the city of Fortaleza, State of Ceará (Brazil). He received the B.S. degree in Physics from the Federal University of Ceará (1980). The M.Sc. (1983) and D.Sc. (1992) degrees both in Biomedical Engineering were obtained in the Federal University of Rio de Janeiro (UFRJ). Since Septembre/1992, he has a position as a Lecturer/Researcher at the Biomedical Engineering Program –COPPE/UFRJ. His main research fields of interest are Biomedical Ultrasound Image and signal processing, tissue characterization and Clinical Engineering applied to medical ultrasound.

Antonio Fernando Catelli Infantosi

Received his Ph.D. from Imperial College of Science, Technology & Medicine - University of London, UK, in 1986. He is currently Professor of Biomedical Signal Processing of the Post-Graduate Engineering Institution (COPPE/UFRJ). His main research interests are in Neural Engineering, Image Processing and biological phenomenon (neural) modelling. He had already published 83 papers in different recognized journals, ten book chapters, nearly 330 papers in congress and he was the supervised of 19 PhD thesis and 48 masters.